A Comparison of Two Conformal Methods for FDTD Modeling

Mark W. Steeds
Shira L. Broschat
John B. Schneider
School of Electrical Engineering and Computer Science
Washington State University
Pullman, WA 99164-2752

CORRESPONDENCE:
Mark W. Steeds
Electrical Engineering and Computer Science
Washington State University
Pullman, WA 99164-2752
(509) 335-0903
FAX (509) 335-3818
email: msteeds@eecs.wsu.edu

Abstract

Two conformal Finite-Difference Time-Domain (FDTD) methods are considered, which eliminate the effects of the stair-step approximation inherent at low points per wavelength (PPW). The first, proposed by Jurgens *et al.* [*IEEE Trans. Antennas Propagat.*, 40, 357–366, 1992], uses the contour path method. The second, proposed by Yee *et al.* [*IEEE Trans. Antennas Propagat.*, 40, 1068–1075, 1992], uses overlapping grids. Both TE and TM electromagnetic scattering from a two-dimensional (2-D), perfectly-conducting circular cylinder are used to test the accuracy of modeling curved surfaces. Radar cross section results are presented for a circular cylinder with a radius of half a wavelength. Also, TE and TM electromagnetic scattering from a 2-D, perfectly-conducting rotated square cylinder are used to test the accuracy of modeling corners and edges. Radar cross section results are presented for a rotated square cylinder with the length of one side equal to a wavelength. It is shown that the conformal method proposed by Yee *et al.* provides significant improvement in accuracy over the original FDTD algorithm at low PPW for all geometries studied in this paper. Implementation of this method was not difficult for the geometries studied in this paper, but implementation becomes more difficult as geometries become more complex. The conformal method proposed by Jurgens *et al.* provides significant improvement in accuracy over the original FDTD algorithm at low PPW for most of the geometries studied in this paper. However, improvement did not occur for the TM case when the positioning of the rectangular cylinder was such that its corners could not be modeled accurately. Implementation of this method was not difficult and should not increase as the geometries become more complex. In general, the results for the conformal method proposed by Yee *et al.* are more accurate than those for the conformal method proposed by Jurgens *et al.*

I. Introduction

With the advent of powerful and inexpensive computers, the Finite-Difference Time-Domain (FDTD) algorithm, originally proposed by Yee [1], has been used to solve numerous electromagnetic scattering problems in such diverse areas as optics, biomedicine, oceanography, and radar remote sensing. However, because of its stair-step approximation, the original Yee algorithm can give inaccurate results for surfaces that cannot be aligned with the grid, unless a relatively dense grid is used [2]-[3]. Such surfaces include those with curvature and those with rotated edges. Since surfaces with these characteristics are of interest to researchers, several conformal methods have been proposed to address this problem [4]-[12].

This paper presents a comparison of two of the conformal methods that have been proposed. These two are of interest because changes from the rectangular FDTD algorithm are required only in the vicinity of a scatterer. The first, proposed by Jurgens *et al.* [4]-[5], uses the contour path method. In this method only those FDTD cells adjacent to a scatterer are distorted to conform with its geometry. The second, proposed by Yee *et al.* [6]-[7], uses overlapping grids, the original FDTD grid and a grid that conforms to the geometry of a scatterer. Interconnection of the grids is accomplished using interpolation.

The purpose of a conformal FDTD algorithm is to facilitate accurate modeling of curved surfaces while retaining the ability to accurately model corners and edges. Both TE and TM electromagnetic scattering from a two-dimensional (2-D), perfectly-conducting circular cylinder are used to test the accuracy of modeling curved surfaces. Radar cross section results are presented for a circular cylinder with a radius of half a wavelength. Also, TE and TM electromagnetic scattering from a 2-D, perfectly-conducting rotated square cylinder are used to test the accuracy of modeling corners and edges. Radar cross section results are presented for a rotated square cylinder with the length of one side equal to a wavelength. The advantages and disadvantages of both conformal methods are discussed in terms of accuracy, complexity of implementation, and actual improvement over the original FDTD algorithm.

In the next section, the modeling of 2-D, perfectly-conducting objects using the original FDTD algorithm and the two conformal FDTD algorithms is described. In Section III, far-field numerical results for simulations of electromagnetic scattering problems are presented.

II. FDTD Algorithms

The FDTD algorithm is a numerical solution of Maxwell's equations. Equations discretized in space and time are derived from Ampere's and Faraday's Laws. In this section, the modeling of 2-D, perfectly-conducting objects using the original Yee, or uniform, FDTD (UFDTD), the contour path FDTD (CPFDTD), and the conformal FDTD with overlapping grids (CFDTD) is presented.

A. The UFDTD Method

The equations for the UFDTD method are derived from the differential form of the curl equations given by Ampere's and Faraday's Laws in conjunction with the constitutive relations $\mathbf{B}=\mu\mathbf{H}$ and $\mathbf{D}=\epsilon\mathbf{E}$. The 2-D UFDTD grid is defined by square cells of length $\Delta x = \Delta y = \Delta$. The orientation of electric and magnetic field components within a square cell is shown in Fig. 1 for TM_z and TE_z cases. Development of the discretized UFDTD equations can be found in [13]. For a perfect electric conductor the values of all electric field components whose coordinates lie within the conductor are set to zero. However, for the magnetic field the boundary is not well-defined, and a magnetic field component is considered inside the conductor only if all the electric field components used in its calculation are inside. Otherwise, it is considered outside the conductor, even if its coordinates lie inside. As shown in Fig. 1, the locations of the outermost field components that are electrically inside the

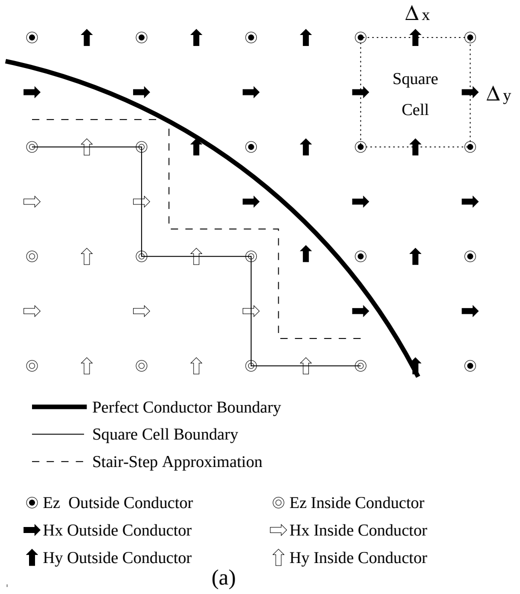

Figure 1: The UFDTD stair-step approximation of the surface of a perfect electric conductor. (a) TM_z case. (b) TE_z case.

conductor define a square cell boundary. The resulting stair-step approximation of the surface of the perfect electric conductor can be assumed to extend $\frac{1}{4}\Delta$ out from this square cell boundary [13, pp. 40–41].

B. The CPFDTD Method

The equations for the CPFDTD method are derived from the integral forms of Ampere's and Faraday's laws together with the constitutive relations [4]-[5]. The discretization of the electric and magnetic field components in both space and time is the same as for the UFDTD method for both the TM_z and TE_z problems, and in regions where no curved media interfaces exist, the equations reduce to those of the UFDTD method.

In regions that contain curved media interfaces, the CPFDTD algorithm of Jurgens *et al.* yields equations that are distinct from those of the UFDTD method. The rectangular contour used in calculating Faraday's Law is distorted to conform to the geometry of the interface. The rectangular contour used in calculating Ampere's Law is not distorted and any contour intersected by a media interface is not used. For the TM_z problem, because the Ampere contours are not distorted, several of the electric field components around the perfect conductor are unused. Magnetic field components not needed in any Ampere contour calculation are also unused. Calculation of the magnetic field components whose Faraday contours are intersected by the perfect conductor is accomplished by shrinking the contour to fit the surface of the conductor. This is shown in Fig. 2(a) and the resulting equation for the H_y field component is

$$H_y^{n+\frac{1}{2}}(i+\frac{1}{2},j) \quad = \quad H_y^{n-\frac{1}{2}}(i+\frac{1}{2},j) + \frac{\Delta t}{l\mu} E_z^n(i+1,j) \tag{1}$$

where i and j are integer indices used to increment spatial coordinates and n is an integer index used to increment time. Magnetic field components whose contours are not intersected by the surface but whose Faraday contours contain unusable electric field components are

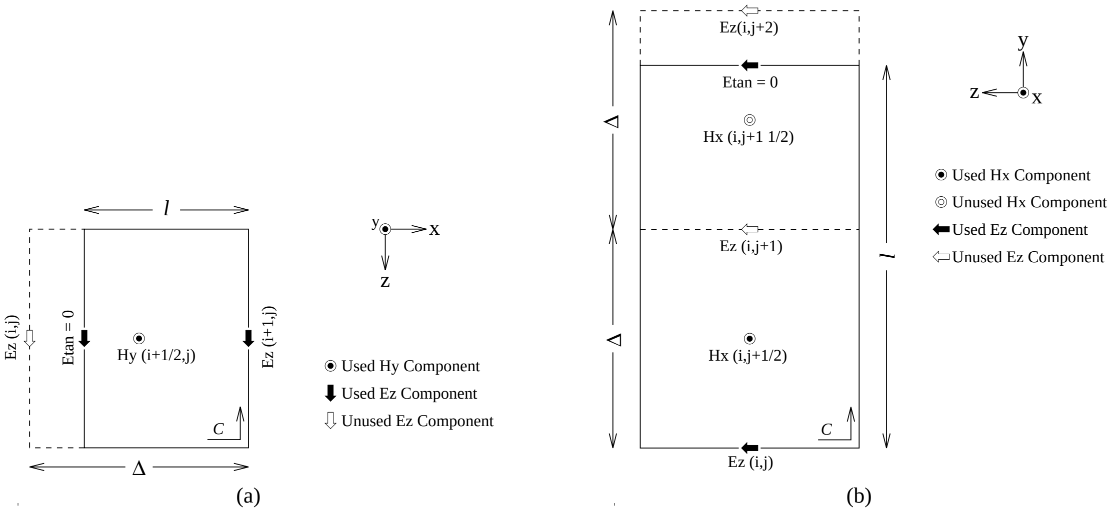

Figure 2: Faraday contours used in the TM_z problem by the CPFDTD method to calculate magnetic field components near the surface of a perfect electric conductor. (a) Shrunken contour used to calculate an H_y component. (b) Extended contour used to calculate an H_x component.

extended to fit the surface of the conductor or else to the next usable electric field component. This is shown in Fig. 2(b) and the resulting equation for the H_x field component is

$$H_x^{n+\frac{1}{2}}(i,j+\frac{1}{2}) = H_x^{n-\frac{1}{2}}(i,j+\frac{1}{2}) + \frac{\Delta t}{l\mu}E_z^n(i,j) \tag{2}$$

For the TE$_z$ problem, electric field components whose corresponding Ampere contours are intersected by the media interface are not used. They are either replaced in calculations by a colinear neighbor on the same side of the interface or ignored. A uniform Faraday contour that contains unusable electric field components is distorted to fit the geometry of the surface. For example, in Fig. 3, contour C_1 ignores the unusable E_x field which is replaced by the zero-valued tangential electric field along the surface of the perfect conductor. The resulting equation for the magnetic field component, H_z, is

$$\begin{aligned} H_z^{n+\frac{1}{2}}(i+\frac{1}{2},j+\frac{1}{2}) &= H_z^{n-\frac{1}{2}}(i+\frac{1}{2},j+\frac{1}{2}) \\ &+\frac{\Delta t}{A_1\mu}\Big(l_2E_y^n(i+1,j+\frac{1}{2}) - l_1E_y^n(i,j+\frac{1}{2}) \\ &-\Delta E_x^n(i+\frac{1}{2},j+1)\Big) \end{aligned} \tag{3}$$

where A_1 is the area within contour C_1. In contour C_2, the contour is again distorted to include the zero-valued tangential electric field, ignoring the unusable E_x component. The unusable E_y component is replaced by its colinear neighbor for the portion of the contour represented by length l_3. The resulting equation is given by replacing l_1 with l_3, l_2 with l_4, and A_1 with A_2 (the area within contour C_2) in (3). In the calculation involving contour C_3, the value of the usable E_y field component along the length l_5 is used for the entire length l_5 since the other E_y field component is unusable. The resulting equation is given by replacing l_1 with l_4, l_2 with l_5, and A_1 with A_3 (the area within contour C_3) in (3).

C. The CFDTD Method

The CFDTD method uses overlapping grids to analyze a scatterer [6]. Grids that conform

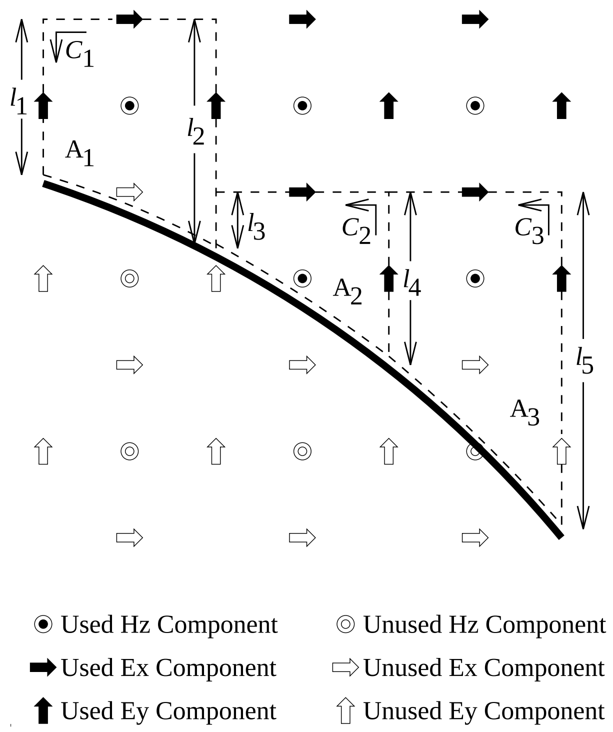

Figure 3: Faraday contours used in the TE_z problem by the CPFDTD method to calculate magnetic field components near the surface of a perfect electric conductor.

to the surface of the scatterer are used in the vicinity of the scatterer. More than one conformal grid may be used if the surface cannot be defined by a single conformal grid. An example of such a surface is one that has a region with curvature and a region without curvature that doesn't align with the rectangular grid. For each grid, FDTD equations are derived from the integral forms of Ampere's and Faraday's Laws together with the constitutive relations. The UFDTD grid is used everywhere except in the immediate vicinity of the scatterer. Information is passed between the conformal and uniform grids using interpolation. The grid systems used may be rectangular, curvilinear, or irregular. Also, there is no requirement that they be orthogonal. Examples of the development of non-rectangular FDTD equations exist in the literature. Holland has derived FDTD equations for the spherical grid system [11] as well as for a general nonorthogonal grid system for which a metric exists [10]. Fusco has also developed an FDTD equation system for curvilinear coordinates [9]. For irregular surfaces such as those encountered in rough surface scattering, Chan *et al.* have developed an irregular grid system for use with the CFDTD method [14].

For illustrative purposes, the implementation of the CFDTD method for a perfectly conducting infinite circular cylinder is described. A cylindrical grid conforms to the surface of such a cylinder. For a single grid cell, as shown in Fig. 4, the radial incremental length $\Delta\rho$ is set equal to the incremental length Δ of the UFDTD grid. For numerical stability, the incremental angle $\Delta\phi$ is chosen so that cylindrical and uniform grid cells are roughly the same size in regions where interpolation is necessary. If $\Delta\phi$ is too small, too many cylindrical grid nodes lie within a rectangular grid cell, leading to instability. Likewise, if $\Delta\phi$ is too large, too many rectangular grid nodes lie within a cylindrical grid cell, again leading to instability. The cylindrical grid extends 3Δ from the surface of the perfect conductor. All UFDTD grid cells whose centers are within a radius equal to the radius of the scattering

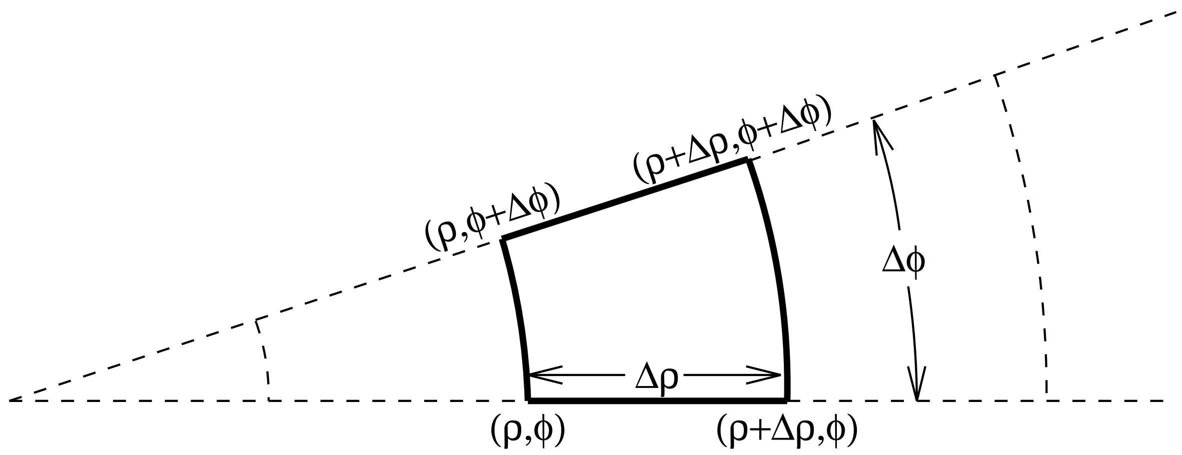

Figure 4: Single grid cell for the cylindrical grid system.

cylinder plus 1.25Δ are not used. The resulting overlapping grid system is shown in Fig. 5 for one quadrant.

Information is exchanged between grids and boundary conditions are enforced in the following manner. For the cylindrical grid, all electric field components positioned on the inner radius are set to zero. This enforces the boundary condition at the perfect conductor–free space interface. Electric field components lying on the outer boundary are interpolated from electric field components in the uniform grid. The remaining electric field components are calculated using cylindrical FDTD equations. Magnetic field components are calculated using cylindrical FDTD equations unless it is possible to interpolate them from magnetic field components in the uniform grid. In this case, a magnetic field component is set equal to the average value of the calculation and interpolation. For the uniform grid, the electric field components lying on the inner boundary are interpolated from electric field components in the cylindrical grid. All other electric field and all magnetic field components are calculated using the UFDTD equations. A cylindrical component is interpolated from its

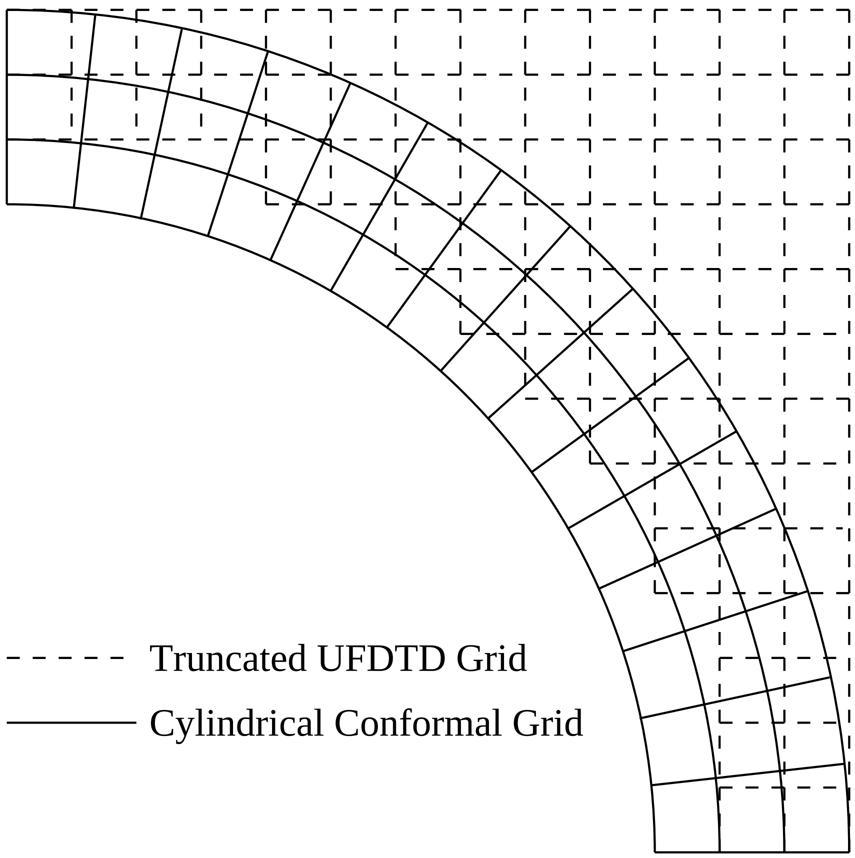

Figure 5: One quadrant of the overlapping rectangular and cylindrical grid systems used in the CFDTD method to model the surface of a perfectly conducting circular cylinder.

four neighboring uniform components. The interpolations in both the x and y directions are linear. Similarly, a uniform component is interpolated from its four neighboring cylindrical components. The interpolations in the ρ direction are linear and those in the ϕ direction are linear along cylindrical segments with ρ held constant.

III. Numerical Results

To test the accuracy of the three FDTD algorithms under consideration, simulations were performed for both TM_z and TE_z cases. Except in the immediate vicinity of scattering bodies, implementation of the three FDTD algorithms were identical so that differences in results could be attributed directly to the algorithms themselves. A total-field formulation was used and third-order Liao absorbing boundary conditions [15] were implemented at the outer boundary of the computational domain. The scatterer was harmonically illuminated by a Gaussian-tapered plane wave with an amplitude given by $(1 - \exp(-\tau t^2))u(t)$, where $u(t)$ is the unit step function. With τ set so that the amplitude of the incident field reaches its maximum after propagating for 10 complete cycles or periods, transients were absent within 15 cycles. After 15 cycles, a near-field to far-field transformation was performed to determine the radar cross section of the scatterer [16]. Radar cross sections for perfectly-conducting circular cylinders and rotated square cylinders were determined. The circular cylinder was chosen to study curved surfaces; the rotated rectangular cylinder was chosen to study corners and edges that do not align with the uniform grid. Rotation angles of 15° and 30° for the square cylinder illustrate the differences in implementation of the three methods. The cylinder sizes were chosen in the resonance region. The radar cross section results were normalized with respect to the wavelength. Insight gained from these simulations can be extended to objects with similar surface characteristics such as ellipses and wedges.

For low values of grid points per wavelength (PPW), the error due to the stair-step approximation of the UFDTD method may produce unacceptable results for objects that do not match the rectangular grid [3]. As the value of PPW is increased, the significance of the stair-step approximation is reduced. It becomes negligible for large values of PPW [3]. A logarithmic ratio is used to compare FDTD results with reference results. For the comparisons in this paper, the reference result is an exact series solution, a moment method solution, or a UFDTD solution at a large value of PPW. For a specific angle, θ, this ratio is defined as

$$\mathrm{E}(\theta) = 10 \times |\log_{10}(\sigma_{\mathrm{FDTD}}(\theta)/\sigma_{\mathrm{reference}}(\theta))| \tag{4}$$

where σ is the radar cross section. The average over all angles defined as

$$\mathrm{E}_{\mathrm{ave}} = \sum_{\theta=1}^{360} \frac{\mathrm{E}(\theta)}{360} \tag{5}$$

Thus, the smaller this ratio, the more accurate the approximate solution is. The logarithmic ratio for the average over all angles of the UFDTD solution for the TM_z radar cross section of the circular cylinder at 160 PPW over the exact series solution is 0.059. However, this accuracy comes at the high cost of using 160 PPW. The purpose of conformal FDTD algorithms is to increase the accuracy at low values of PPW; thus all simulations were performed at 20 PPW. Using the circular cylinder, radar cross section results for the three methods are compared with the exact series solutions. Since no exact theoretical solution exists for the rotated square cylinder, these results are compared with the UFDTD solution obtained at 160 PPW. (The TM_z UFDTD results obtained at 160 PPW for the rotated square cylinders were also compared with moment method results to insure their accuray. The logarithmic ratio in the average over all angles for the 15° rotation is 0.078 and for the 30° rotation is 0.061.) Results from the simulations are plotted in Figs. 6–11. All angles refer to counter-clockwise rotation from the positive x axis. The incident wave propagates in the negative x

direction. The backscattering angle is $0°$ and the forward scattering angle is $180°$. Rotation of the square cylinder is counterclockwise. Logarithmic ratios for the average over all angles, the backscattering angle, and the forward scattering angle are listed in Table 1. In comparing the different methods, attention will be focused on the average ratio. Also, improvements gained using conformal methods are not the same as increasing the PPW of the UFDTD method where convergence toward the exact solution is expected at each angle. The ratios given in Table 1 for the backscattering and forward scattering angles demonstrate this. An explanation and comparison of the results follow.

A. $\mathbf{TM}_z$ Results

In Fig. 6, the radar cross section for the circular cylinder is shown. The radar cross sections for the square cylinders rotated $15°$ and $30°$ are shown in Figs. 7 and 8, respectively. An analysis of Figs. 6 and 7 and Table 1 shows that the CPFDTD method provides noticeable improvement over the UFDTD method for the circular cylinder and for the square cylinder rotated $15°$ for E_{ave}. However, as shown in Fig. 8 and Table 1, there is significantly less improvement in E_{ave} for the square cylinder rotated $30°$. The discrepancy between the rotations of $15°$ and $30°$ is due to the positioning of the corners of the cylinder in relation to the rectangular grid. The Faraday contours for the TM_z problem are positioned in the x-z and y-z planes while the surface is described in the x-y plane. This results in the surface being modeled at discrete points spaced Δ apart. For the $15°$ rotation, the distortion of Faraday contours near the corners provides a good model of the corners. For the $30°$ rotation, the positioning of the corners in relation to the rectangular grid does not allow the distorted Faraday contours to provide an accurate model of the corners. Thus, the CPFDTD algorithm is still dependent on the positioning of the scatterer in relation to the rectangular grid. Corners and similar surface discontinuities may result in problems in the CPFDTD modeling

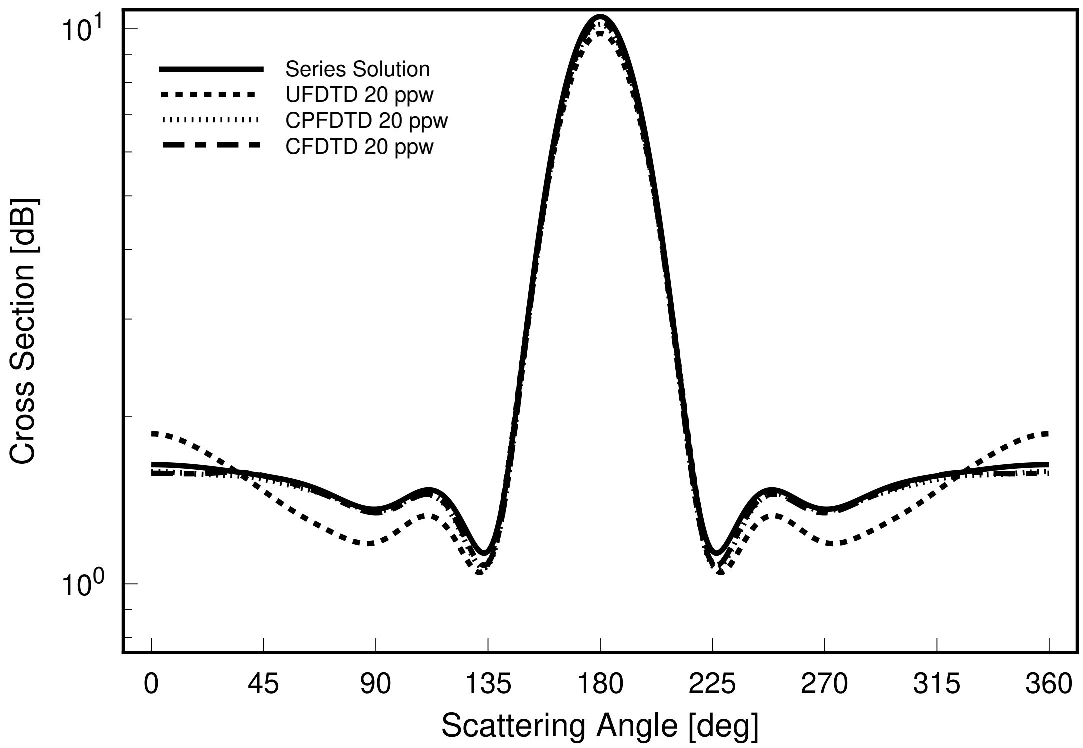

Figure 6: Radar cross sections for the UFDTD, CPFDTD, and CFDTD methods at 20 PPW and an exact series solution for a TM_z perfectly conducting circular cylinder with a radius of half a wavelength. Here and in Figs. 7, 9, 10, and 11 the CPFDTD and CFDTD methods give improved results over the UFDTD method.

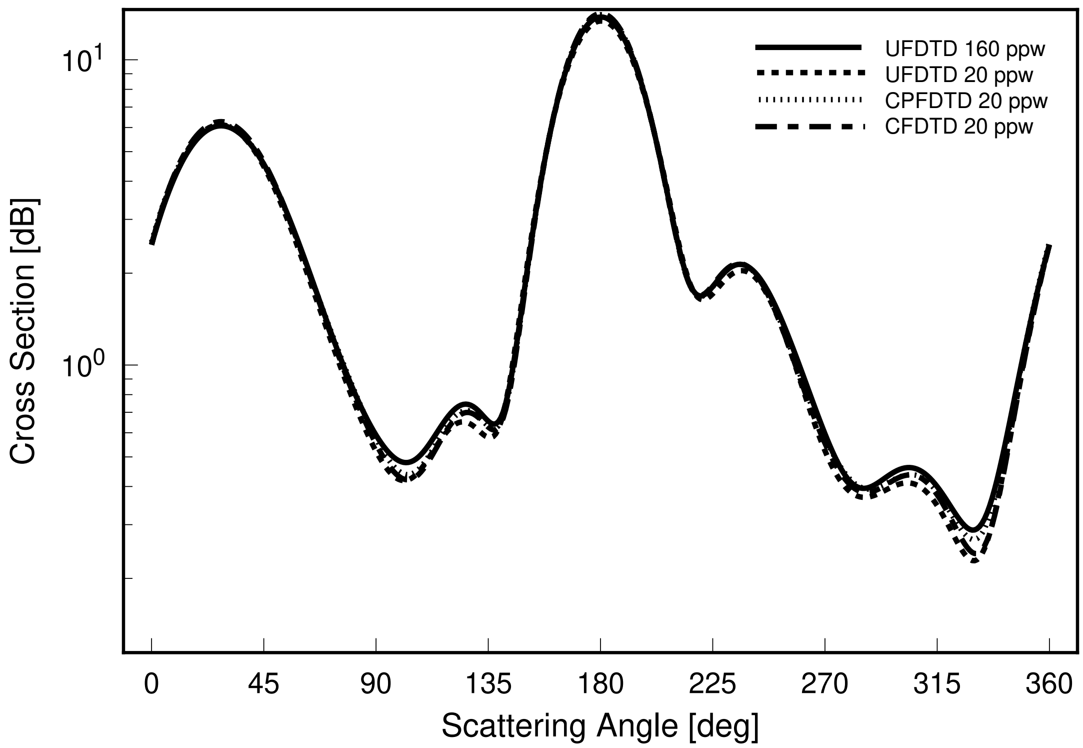

Figure 7: Radar cross sections for the UFDTD, CPFDTD, and CFDTD methods at 20 PPW and the UFDTD method at 160 PPW for a TM_z perfectly conducting square cylinder rotated 15° with the length of one side equal to a wavelength.

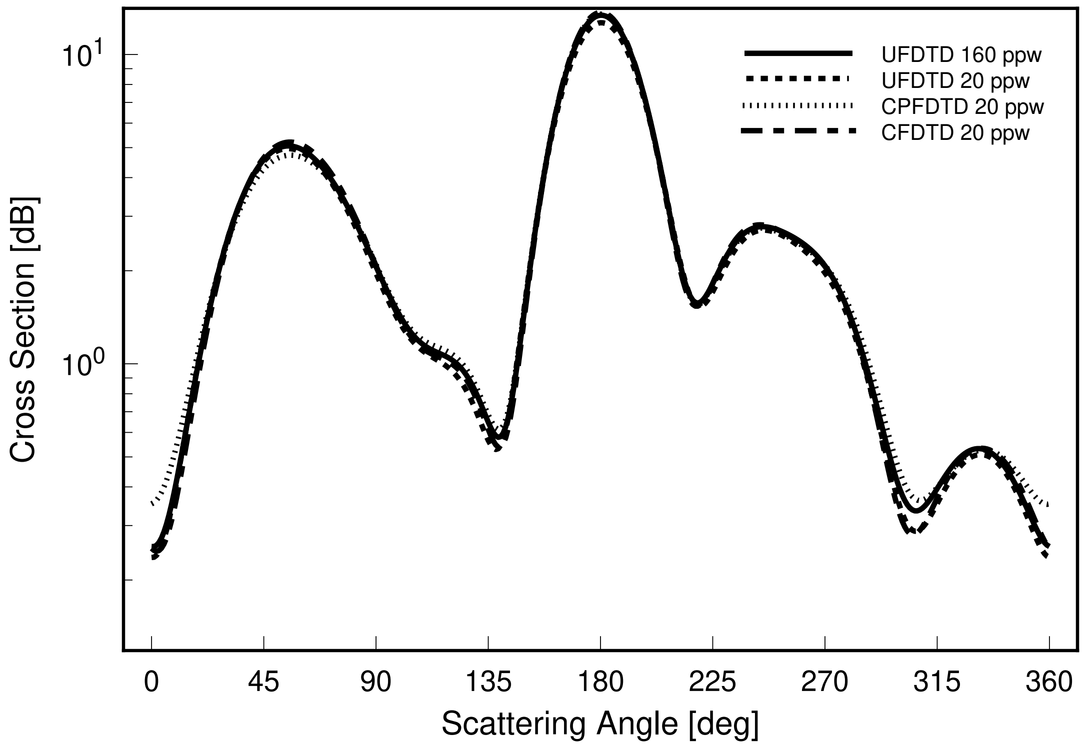

Figure 8: Radar cross sections for the UFDTD, CPFDTD, and CFDTD methods at 20 PPW and the UFDTD method at 160 PPW for a TM_z perfectly conducting square cylinder rotated 30° with the length of one side equal to a wavelength. Here the CFDTD method gives improved results over the UFDTD method but the CPFDTD method does not because the CPFDTD method still depends on the positioning of the scatterer in relation to the rectangular grid for the TM_z case. However, the CFDTD method cannot always be used (see text); whereas the CPFDTD method is not restricted.

of surfaces.

An analysis of Figs. 6–8 and Table 1 shows that the CFDTD method provides noticeable improvement over the UFDTD method for the circular cylinder and both rotations of the square cylinder for E_{ave}. Unlike the CPFDTD method, the CFDTD method does not depend on the positioning of the scatterer in relation to the rectangular grid to define the surface of the scatterer. This is demonstrated by the similarities in E_{ave} for the CFDTD results as compared with the volatility shown in E_{ave} for the CPFDTD results for the different angles of rotation of the square cylinder. Simulations were also run for a circular cylinder with a radius of a tenth of a wavelength, and average ratios similar to those of Table 1 were obtained.

B. TE$_z$ Results

In Fig. 9, the radar cross section for the circular cylinder is shown. The radar cross sections for the square cylinders rotated 15° and 30° are shown in Figs. 10 and 11, respectively. An analysis of Figs. 9–11 and Table 1 shows that both the CPFDTD and CFDTD methods give significant improvement over the UFDTD method for the circular cylinder and both rotations of the square cylinder for the average over all scattering angles. Since the Faraday contours of the CPFDTD are in the x-y plane, they can be distorted to accurately model corners and similar irregularities. The problems encountered with CPFDTD modeling in the TM$_z$ problem do not arise in the TE$_z$ problem. Simulations were also run for a circular cylinder with a radius of a tenth of a wavelength, and average ratios similar to those of Table 1 were obtained.

In general, the TE$_z$ UFDTD results are not as accurate as corresponding TM$_z$ UFDTD results for the same surface geometry. The discrepancy is due to difficulties in exciting surface current in the TE$_z$ problem [3],[13]. Current is excited on the surface of a perfectly-

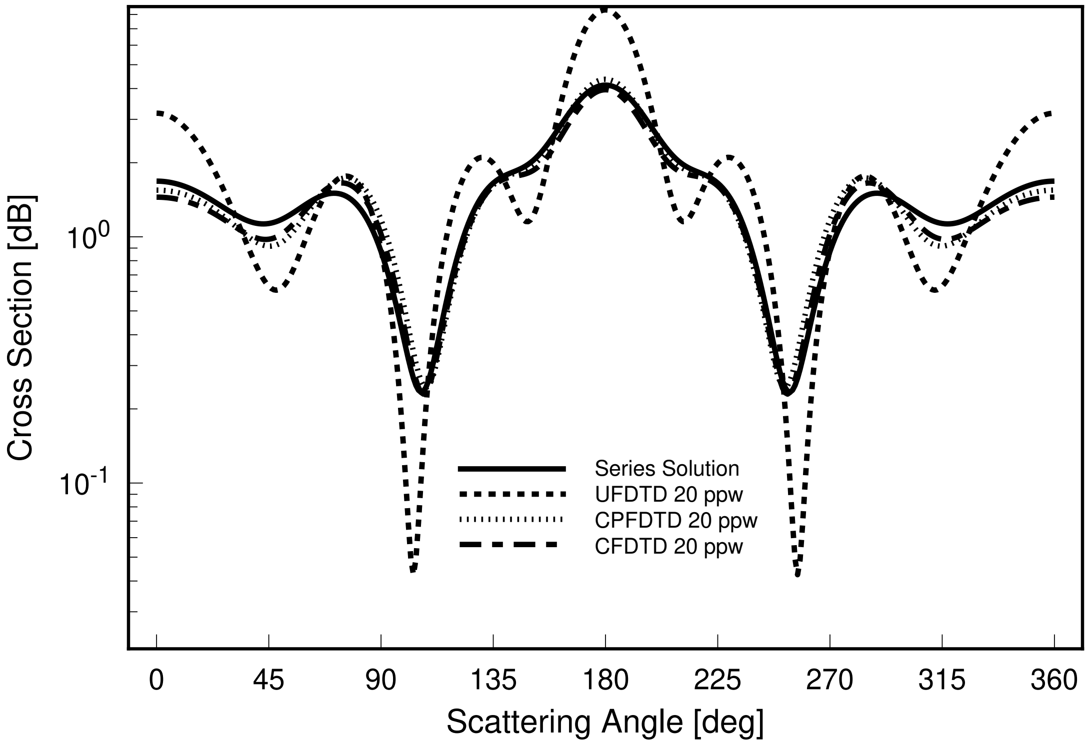

Figure 9: Radar cross sections for the UFDTD, CPFDTD, and CFDTD methods at 20 PPW and an exact series solution for a TE_z perfectly conducting circular cylinder with a radius of half a wavelength.

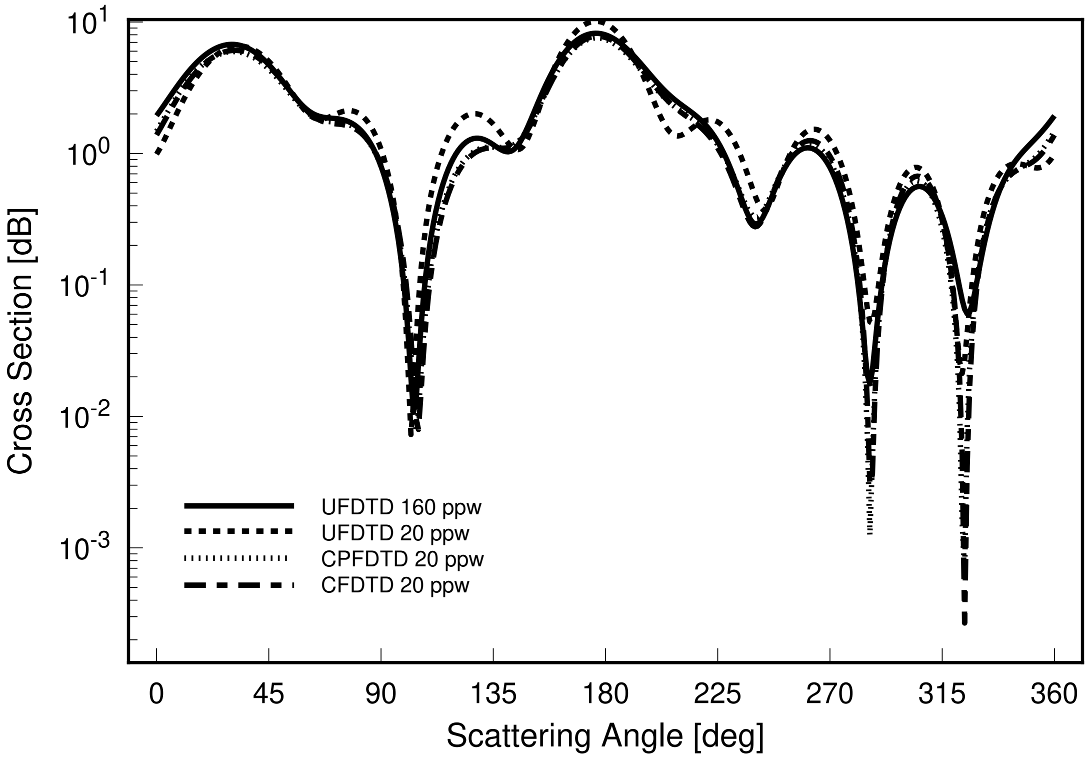

Figure 10: Radar cross sections for the UFDTD, CPFDTD, and CFDTD methods at 20 PPW and the UFDTD method at 160 PPW for a TE_z perfectly conducting square cylinder rotated 15° with the length of one side equal to a wavelength.

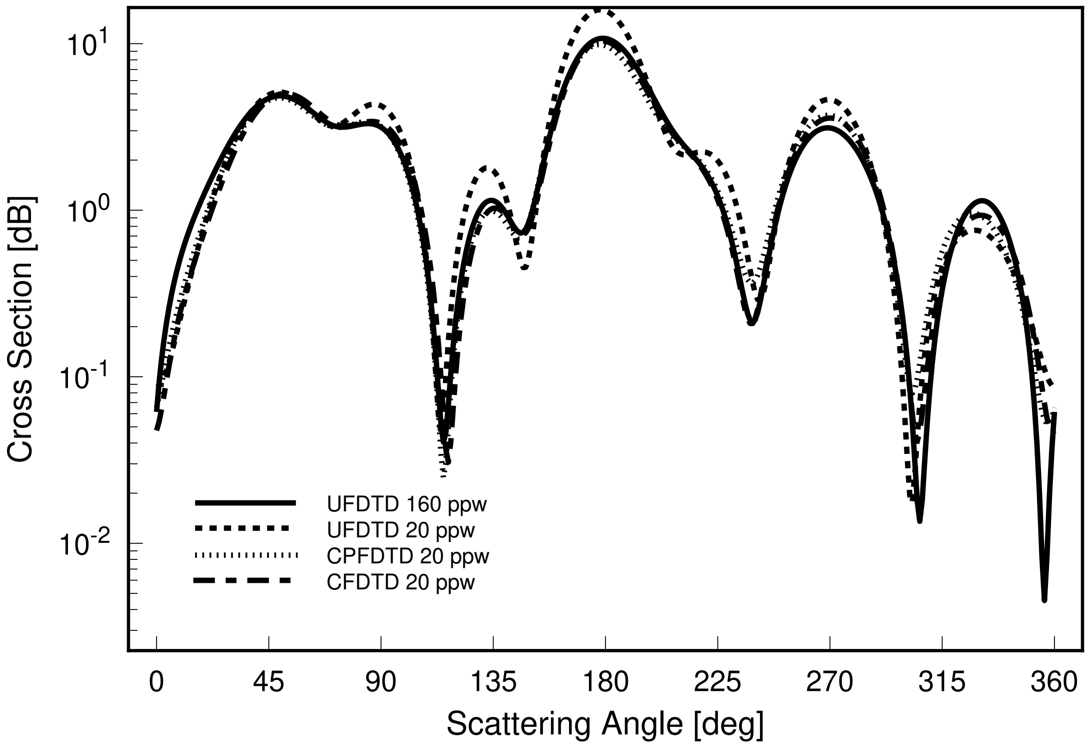

Figure 11: Radar cross sections for the UFDTD, CPFDTD, and CFDTD methods at 20 PPW and the UFDTD method at 160 PPW for a TE_z perfectly conducting square cylinder rotated 30° with the length of one side equal to a wavelength.

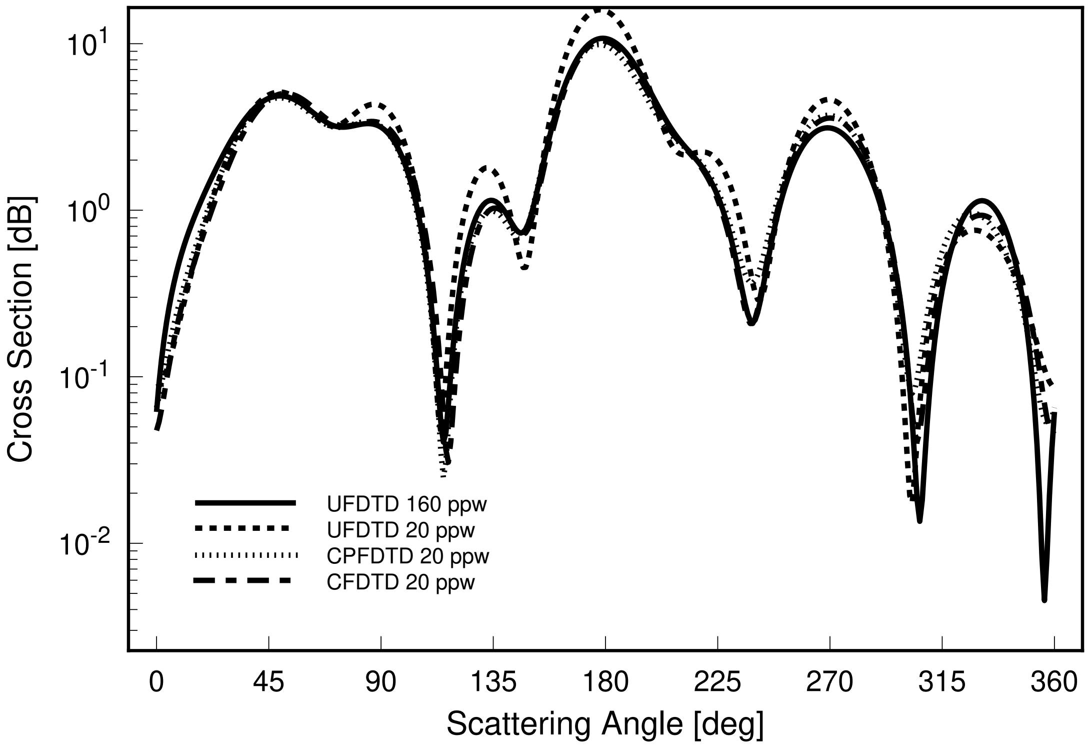

Figure 12: Radar cross sections for the UFDTD, CPFDTD, and CFDTD methods at 20 PPW and the UFDTD method at 160 PPW for a TE_z perfectly conducting square cylinder rotated 30° with the length of one side equal to a wavelength.

conducting object by an incident electric field parallel to the object's surface. For the TM_z problem, the incident electric field component, E_z, is always parallel to the surface and the stair-step approximation does not affect the excitation of current. However, the incident electric field for the TE_z problem, E_y, is not necessarily parallel to the surface and excitation of current is dependent on the stair-step approximation. Although the TE_z CPFDTD and CFDTD results are not as accurate as corresponding TM_z results for identical geometries, the improvement over the UFDTD results is generally the same for TE_z as for TM_z.

IV. Discussion

Of the three methods presented, the UFDTD method is the easiest to implement. Knowledge of the position of the electric field components in relation to the surface of a perfectly conducting object is all that is required for its modeling. However, the stair-step approximation that results can give unacceptable results at low PPW. Accurate results come at the expense of the increased computer time needed for higher values of PPW.

The CFDTD method yields a significant improvement in accuracy over the UFDTD method at low PPW for all the geometries studied in the previous section. This improvement comes at the expense of increased difficulty in implementation. FDTD equations for grids that conform to the surface of the scattering object must be derived and a successful coupling between grids used must be developed. For the simple canonical objects studied in this paper, the increase in accuracy justifies the modest increase in implementation complexity. However, the complexity of the implementation increases with the complexity of the surface. Also, surfaces exist for which implementation of the CFDTD algorithm is unmanageable—for example, surfaces that have concavities that are too small to permit the construction of a conformal grid system. Since the CFDTD method has been shown to be effective in modeling curved surfaces, corners, and edges [6]-[7],[14], it is recommended for those surfaces for which implementation is manageable.

The CPFDTD method yields a significant improvement in accuracy over the UFDTD method at low PPW for most of the geometries studied in the previous section. Madsen has raised questions about the second-order accuracy and long term stability of the CPFDTD method [17]. However, no such difficulties arose in this study. Increased difficulty in implementation occurs because knowledge of the position of all field components and the contour of integration in relation to the surface of an object is required for its use. For the TM_z problem, the usefulness of the CPFDTD method depends on the characteristics of the surface being modeled. The increased accuracy should outweigh the increased implementation complexity for all surfaces that do not have corners or discontinuities that cannot be accurately modeled because of the spacing of the rectangular grid. For the TE_z problem, the accuracy of the CPFDTD method justifies the increased difficulty in implementation. Although there are cases for which the CPFDTD method gives better accuracy than the CFDTD method, the CFDTD method generally gives more accurate results. However, as the complexity of the surface is increased, the implementation of the CPFDTD method does not increase in difficulty. Therefore, surfaces whose implementation by the CFDTD method is unmanageable can be modeled using the CPFDTD method.

A few comments can be made regarding the implementation of both the CFDTD and CPFDTD methods for three-dimensional scattering bodies. The CFDTD method should provide better results than the CPFDTD method since it globally conforms to the surface of the object. The CPFDTD method only samples or models the surface at planes spaced Δ apart. The difficulties in implementation will increase considerably for both methods over the 2-D case. As in the 2-D case, the difficulty in implementing the CFDTD method will increase with the complexity of the scattering body. The difficulty in implementing the CPFDTD method should not increase with changes in the complexity of the scattering body.

Table 1: Logarithmic comparison of FDTD results and reference results. Ratios are given for the average over all angles, the backscattering angle (θ=0°), and the forward scattering angle (θ=180°).

Scattering Object	Algorithm	E_{ave}	E(θ=0°)	E(θ=180°)
TM_z circular cylinder	UFDTD	.38	.56	.31
	CPFDTD	.11	.12	.14
	CFDTD	.093	.16	.096
TM_z rotated square cylinder (15°)	UFDTD	.30	.002	.13
	CPFDTD	.11	.085	.074
	CFDTD	.20	.002	.11
TM_z rotated square cylinder (30°)	UFDTD	.21	.35	.24
	CPFDTD	.21	1.4	.034
	CFDTD	.16	.058	.091
TE_z circular cylinder	UFDTD	1.8	2.8	3.1
	CPFDTD	.49	.37	.23
	CFDTD	.42	.65	.19
TE_z rotated square cylinder (15°)	UFDTD	1.4	2.9	.86
	CPFDTD	.83	1.2	.34
	CFDTD	.89	1.5	.19
TE_z rotated square cylinder (30°)	UFDTD	1.6	1.5	1.7
	CPFDTD	.92	.26	.43
	CFDTD	.88	1.1	.17

Acknowledgment

This work was supported by the National Science Foundation Grant No. ECS9253547.

References

[1] K.S. Yee. Numerical Solution of Initial Boundary Value Problems Involving Maxwell's Equations in Isotropic Media. *IEEE Trans. Antennas Propagat.*, AP-14(4):302–307, 1966.

[2] R. Holland. The Case Against Staircasing. In *6th Annual Review of Progress in Applied Computational Electromagnetics*, pages 89–95, Monterey, CA, March 1990.

[3] R. Holland. Pitfalls of Staircase Meshing. *IEEE Trans. Electromagn. Compat.*, 35(4):434–439, 1993.

[4] T.G. Jurgens, A. Taflove, K. Umashankar, and T.G. Moore. Finite-Difference Time-Domain Modeling of Curved Surfaces. *IEEE Trans. Antennas Propagat.*, 40(4):357–366, 1992.

[5] T.G. Jurgens and A. Taflove. Three-Dimensional Contour FDTD Modeling of Scattering from Single and Multiple Bodies. *IEEE Trans. Antennas Propagat.*, 41(12):1703–1708, 1993.

[6] K.S. Yee, J.S. Chen, and A.H. Chang. Conformal Finite-Difference Time-Domain (FDTD) with Overlapping Grids. *IEEE Trans. Antennas Propagat.*, 40(9):1068–1075, 1992.

[7] K.S. Yee, J.S. Chen, and A.H. Chang. Conformal Finite Difference Time Domain (FDTD) with Overlapping Grids. In *IEEE Antennas and Propagat. Soc. Int. Symposium*, volume 4, pages 1949–1952, Chicago, IL, July 1992.

[8] N.K. Madsen and R.W. Ziolkowski. Numerical Solution of Maxwell's Equations in Time Domain Using Irregular Nonorthogonal Grids. *Wave Motion*, 10(6):583–596, 1988.

[9] M. Fusco. FDTD Algorithm in Curvilinear Coordinates. *IEEE Trans. Antennas Propagat.*, 38(1):76–89, 1990.

[10] R. Holland. Finite Difference Solutions of Maxwell's Equations in Generalized Nonorthogonal Coordinates. *IEEE Trans. Nucl. Sci.*, NS-30(6):4589–4591, 1983.

[11] R. Holland. THREDS: A Finite-Difference Time-Domain EMP Code in 3D Spherical Coordinates. *IEEE Trans. Nucl. Sci.*, NS-30(6):4592–4595, 1983.

[12] J.-F. Lee, R. Palandech, and R. Mittra. Modeling Three-Dimensional Discontinuities in Waveguides Using Non-Orthogonal FDTD Algorithm. *IEEE Trans. Microwave Theory Tech.*, 40(2):346–352, 1992.

[13] K.S. Kunz and R.J. Luebbers. *The Finite Difference Time Domain Method for Electromagnetics*. CRC Press, Boca Raton, FL, 1993.

[14] C.H. Chan, L. Li, J.T. Elson, and L. Tsang. A Conformal Finite-Difference Time-Domain Approach for Monte Carlo Simulations of Random Rough Surface Scattering. In *URSI Digest*, page 13, Chicago, IL, July 1992.

[15] Z.P. Liao, H.L. Wong, B.P. Yang, and Y.F. Yuan. A Transmitting Boundary for Transient Wave Analysis. *Sci. Sin., Ser. A*, 27(10):1063–1076, 1984.

[16] C.A. Balanis. *Advanced Engineering Electromagnetics*. John Wiley & Sons, New York, 1989.

[17] N.K. Madsen. Divergence Preserving Discrete Surface Integral Methods for Maxwell's Curl Equations Using Non-Orthogonal Unstructured Grids. Technical Report UCRL-JC-109787, Lawrence Livermore National Laboratory, 1992. also RIACS Tech. Report 92.04.